



# Martian sub-crustal stress from gravity and topographic models



Robert Tenzer<sup>a,\*</sup>, Mehdi Eshagh<sup>b,c</sup>, Shuanggen Jin<sup>d,e,f</sup>

<sup>a</sup> The Key Laboratory of Geospace Environment and Geodesy, School of Geodesy and Geomatics, Wuhan University, Wuhan, China

<sup>b</sup> Department of Engineering Science, University West, Trollhättan, Sweden

<sup>c</sup> Division of Geodesy and Geoinformatics, Royal Institute of Technology (KTH), Stockholm, Sweden

<sup>d</sup> Shanghai Astronomical Observatory, Chinese Academy of Sciences, Shanghai, China

<sup>e</sup> Department of Geomatics Engineering, Bulent Ecevit University, Zonguldak, Turkey

<sup>f</sup> School of Traffic and Transportation Engineering, Changsha University of Science and Technology, Changsha, China

## ARTICLE INFO

### Article history:

Received 24 October 2014

Received in revised form 20 March 2015

Accepted 25 May 2015

Available online xxxx

Editor: C. Sotin

### Keywords:

crust  
gravity  
impact craters  
Mars  
stress field  
volcanoes

## ABSTRACT

The latest Martian gravity and topographic models derived from the Mars Orbiter Laser Altimeter and the Mars Global Surveyor spacecraft tracking data are used to compute the sub-crustal stress field on Mars. For this purpose, we apply the method for a simultaneous determination of the horizontal sub-crustal stress component and the crustal thickness based on solving the Navier–Stokes problem and incorporating the Vening Meinesz–Moritz inverse problem of isostasy. Results reveal that most of the Martian sub-crustal stress is concentrated in the Tharsis region, with the most prominent signatures attributed to a formation of Tharsis major volcanoes followed by crustal loading. The stress distribution across the Valles Marineris rift valleys indicates extensional tectonism. This finding agrees with more recent theories of a tectonic origin of Valles Marineris caused, for instance, by a crustal loading of the Tharsis bulge that resulted in a regional trusting and folding. Aside from these features, the Martian stress field is relatively smooth with only a slightly enhanced pattern of major impact basins. The signatures of active global tectonics and polar ice load are absent. Whereas the signature of the hemispheric dichotomy is also missing, the long-wavelength spectrum of the stress field comprises the signature of additional dichotomy attributed to the isostatically uncompensated crustal load of Tharsis volcanic accumulations. These results suggest a different origin of the Earth's and Martian sub-crustal stress. Whereas the former is mainly related to active global tectonics, the latter is generated by a crustal loading and regional tectonism associated with a volcanic evolution on Mars. The additional sub-crustal stress around major impact basins is likely explained by a crustal extrusion after impact followed by a Moho uplift.

© 2015 Elsevier B.V. All rights reserved.

## 1. Introduction

Terrestrial sub-crustal stress has been studied in the context of interpreting tectonic and magnetic features, deep earthquake mechanisms, volcanism, subduction, mantle convection, heat flow, kimberlite magmatism and ore concentration. For overview of these studies we refer readers to Eshagh and Tenzer (2014). Runcorn (1964) demonstrated that the sub-crustal stress (caused by mantle convection) can be detected from the gravity field. He derived a functional relation between the gravity field and the sub-crustal stress by means of solving the Navier–Stokes problem and assuming a two-layered Earth's model. The recent progress in developing the gravity and topographic models of planetary bodies

(such as Mars and Venus) allowed studying also the stress field of these planets. Turtle and Melosh (1997), for instance, modeled the lithospheric flexure and stress around Alba Patera on Mars. Dimitrova et al. (2006) compiled the deviatoric lithospheric stress over the Martian western hemisphere using the Mars Orbiter Laser Altimeter (MOLA) topographic model and inferred crustal thickness (Neumann et al., 2004).

The main disadvantage of the Runcorn (1964) definition is a limited spectral resolution of the computed stress field (due to the divergence of an asymptotically-convergent series above a spherical harmonic degree of 25). Moreover, he assumed only a uniform Moho model. To overcome these issues, Eshagh and Tenzer (2014) modified the Runcorn (1964) definition by means of improving a convergence domain of harmonic expansion and considering a variable Moho model. According to their formulation, the Vening Meinesz–Moritz (VMM) inverse problem of isostasy (cf. Sjöberg, 2009) is incorporated in solving the Navier–Stokes problem. In this way, the sub-crustal stress and the crustal thickness (i.e. Moho

\* Corresponding author. Postal address: School of Geodesy and Geomatics, The Key Laboratory of Geospace Environment and Geodesy, Wuhan University, 129 Luoyu Road, Wuhan, 430079, China. Tel.: +86 27 6877 8649; fax: +86 27 6877 1695.

E-mail address: rtenzer@sgg.whu.edu.cn (R. Tenzer).

depth) could be determined directly from gravity and topographic models.

Eshagh and Tenzer (2014) applied this method to investigate a global pattern of the terrestrial sub-crustal stress field. Their result revealed that most of the sub-crustal stress is generated by the inter-plate tectonics, while the intra-plate stress is mainly accumulated along active strike-slip fault systems. Tenzer and Eshagh (in press) investigated distributions and tectonic characteristics of the sub-crustal stress in Taiwan region. They demonstrated that the maximum stress anomalies mark distinctively sections of convergent plate boundaries while the stress intensity attenuates along transform zones and diminishes along divergent zones. They also showed that the oceanic subduction generates the shear stress along the convergent plate boundaries with possibly the additional tensional stress attributed to a back-arc rifting. The shear stress is also generated by the continent-to-continent plate collision (Eshagh and Tenzer, 2014). The geometry of stress vectors indicates the compressional tectonism of orogenic formations and the extensional tectonism of continental basins.

These findings support the concept that most of the Earth's sub-crustal stress is related to active global tectonics caused by mantle convection. This, however, might not be the case for other planetary bodies in the solar system due to their different geological origin and evolution. Recent studies revealed that tectonic features on the Martian surface have a regional character, while there is no evidence of active global tectonics in a more recent geological history of Mars (e.g., Zuber, 2001). A possible presence of the Martian stress field is then likely of a different origin. In this study we investigate some aspects that might bring new evidences for a better understanding of the Martian tectonic evolution. For this purpose, we use the latest gravity and topographic models to evaluate the Martian crustal thickness and the sub-crustal stress field. We derived the Martian Moho model based on solving the VMM inverse problem of isostasy. This isostatic model assumes a regional compensation scheme based on a thin plate lithospheric flexure model. In studies by Zuber et al. (2000) and Neumann et al. (2004) the Martian crustal thickness was determined from gravity and topographic models based on the Airy isostatic model. Since the Airy or Pratt's models assume only a local compensation mechanism, the VMM model should recover the Martian Moho geometry more realistically. We then used information on the crustal thickness to determine the Martian sub-crustal stress. The numerical findings are discussed in the context of currently accepted theories on the Martian history and evolution. The article is organized as follows: The methodology is reviewed in Section 2. The overview of major features of the Martian topography and gravity field is given in Section 3. The numerical results are presented and discussed in Section 4. Major findings are summarized and concluded in Section 5.

## 2. Theoretical model

We applied the method of Eshagh and Tenzer (2014) to determine simultaneously the crustal thickness and the sub-crustal stress field of Mars. The overview of this method is given below.

### 2.1. Sub-crustal stress field

The meridional and prime-vertical components  $S_x$  and  $S_y$  of the sub-crustal stress are defined as (Eshagh and Tenzer, 2014)

$$S_x = \frac{\partial S}{\partial \theta}, \quad S_y = \frac{\partial S}{\sin \theta \partial \lambda}, \quad (1)$$

where a horizontal position is specified by spherical co-latitude  $\theta$  and longitude  $\lambda$ . The stress function  $S$  in Eq. (1) is given by

$$S = \frac{g \Delta \rho^{c/m}}{s^2} \sum_{n=2}^N \frac{1}{(n-1)s^{n+1}} \left[ \frac{2n+1}{n+1} \frac{\rho^c}{2 \Delta \rho^{c/m}} H_n - (D_0)_n \right], \quad (2)$$

where  $g$  is the mean gravity at the planetary surface,  $\Delta \rho^{c/m}$  is a constant value of the crust–mantle (Moho) density contrast,  $\rho^c$  is the average crustal density,  $H_n$  are the Laplace coefficients of topographic heights (defined in Eq. (7)),  $(D_0)_n$  are the Laplace coefficients of Moho depths (defined in Eq. (4)), and  $N$  is the maximum degree of a spherical harmonic expansion. The parameter  $s = 1 - D/R$  is a ratio function of the Moho depth  $D$  and the mean equatorial planetary radius  $R$ . For Mars, we adopted the following values:  $g \cong 3.7 \text{ m/s}^2$  and  $R = 3395.428 \times 10^3 \text{ m}$ . A discussion of values which approximate the crustal density and the crust–mantle density contrast on Mars are postponed until Subsections 3.3 and 4.1 respectively.

The computation of the sub-crustal stress is practically realized in two steps. First, the stress function is computed in a frequency domain to a certain degree of the spectral resolution according to Eq. (2). The numerical differentiation is then applied to evaluate the horizontal components  $S_x$  and  $S_y$  (in Eq. (1)). The variable Moho geometry is determined based on solving the VMM inverse problem of isostasy.

### 2.2. Crustal thickness

Sjöberg (2009) presented an approximate solution (up to the second-order term) to the VMM problem for finding the Moho depth  $D$  in the following form

$$D(\theta, \lambda) = D_0(\theta, \lambda) + \frac{D_0^2(\theta, \lambda)}{R} - \frac{1}{8R} \iint_{\sigma} \frac{D_0^2(\theta', \lambda') - D_0^2(\theta, \lambda)}{\sin^3(\psi/2)} d\sigma', \quad (3)$$

where  $\psi$  is the spherical distance,  $\sigma$  is the unit sphere, and  $d\sigma' = \sin \theta' d\theta' d\lambda'$  is the surface integration element. The spherical harmonic representation of the (nominal) Moho depth  $D_0$  reads

$$D_0 = \sum_{n=0}^N (D_0)_n = -\frac{g_0^i}{4\pi G \Delta \rho^{c/m}} \delta_{n,0} + 2\pi G \kappa_n \rho^c H_n - \kappa_n \Delta g_n, \quad (4)$$

where  $G = 6.674 \times 10^{-11} \text{ m}^3 \text{ kg}^{-1} \text{ s}^{-2}$  is the Newton gravitational constant,  $g_0^i$  is the normal compensation attraction,  $\delta_{n,0}$  is the Kronecker delta, and  $H$  is the topographic height. The parameters  $\{\kappa_n : n = 0, 1, \dots, N\}$  are given by

$$\kappa_n = \frac{1}{4\pi G \Delta \rho^{c/m}} \frac{2n+1}{n+1}. \quad (5)$$

The isostatic compensation attraction  $g_0^i$  in Eq. (4) is computed from Sjöberg (2009)

$$g_0^i = \frac{4\pi}{3} G R \Delta \rho^{c/m} \left[ \left(1 - \frac{D}{R}\right)^3 - 1 \right]. \quad (6)$$

The Laplace harmonics of the topography are defined by the following integral convolution

$$H_n = \frac{1}{4\pi} \sum_{m=-n}^n \iint_{\sigma} H(\theta', \lambda') Y_{n,m}(\theta', \lambda') d\sigma', \quad (7)$$

where  $Y_{n,m}$  are the fully-normalized spherical harmonics.

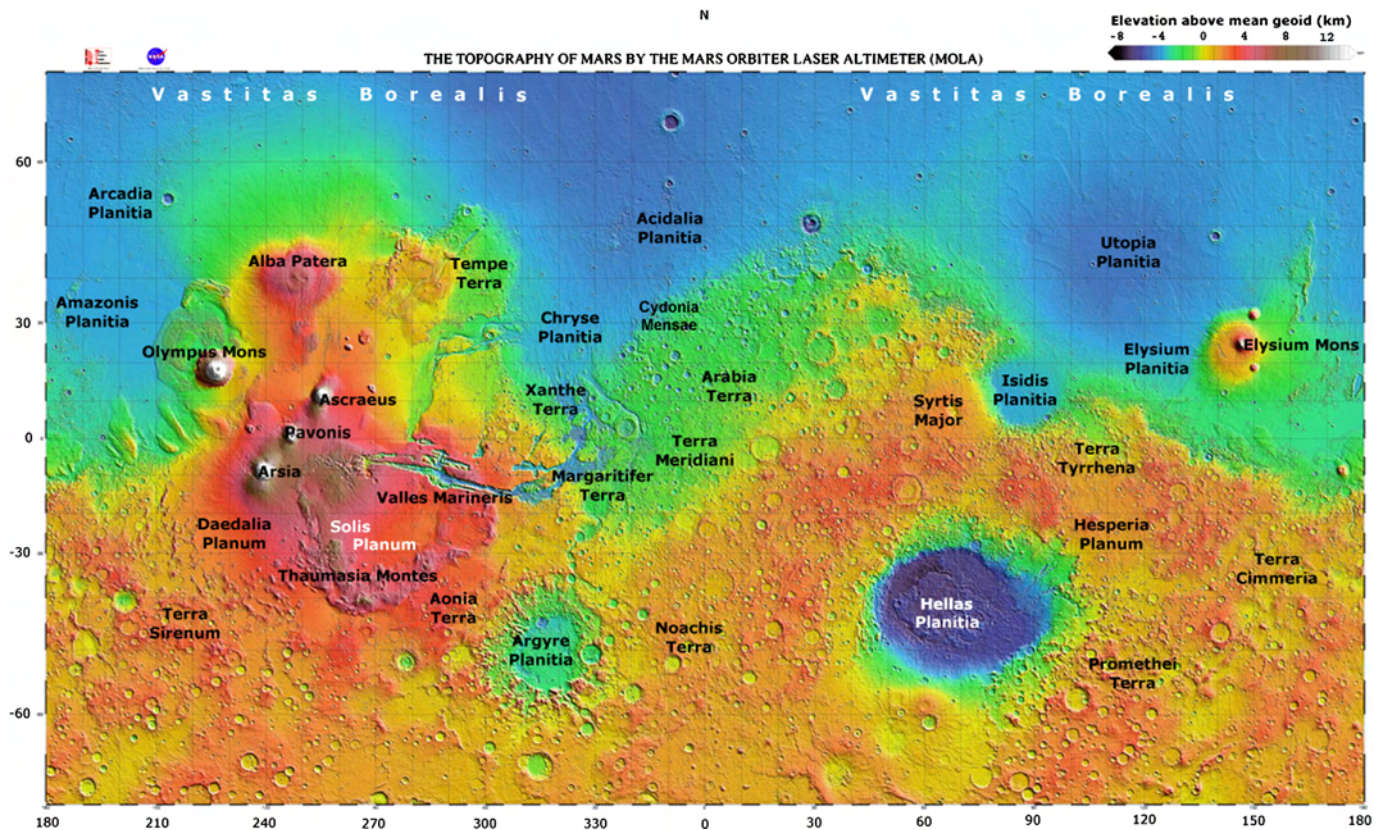


Fig. 1. Geographical description of major topographic features on Mars according Rodrigue CM, Geography, CSULB, 2007 (<http://www.csulb.edu/~rodrigue/mars/MOLAMercatorlabel.jpg>).

The computation of the third constituent on the right-hand side of Eq. (3) is practically realized by limiting the surface integration area over the near zone while disregarding the contribution of the distant zone. The solution of the integral equation in Eq. (3) then gives the Moho depth without applying an iterative procedure. Moreover, the singularity for  $\psi \rightarrow 0$  is solved analytically (Sjöberg, 2009).

### 3. Martian topographic and gravity models

The gravimetric determination of the crustal thickness and the sub-crustal stress is – in principle – realized using gravity and crustal structure models. Since the lithospheric density model of Mars is not yet available, we used only gravity and topographic information while assuming uniform crustal and upper mantle densities.

#### 3.1. Martian topography

We used the MOLA discrete topographic data to generate the coefficients of the Martian global topography complete to a spherical harmonic degree of 85. This spectral resolution is the same as that of the Martian gravity model MRO110B2 used in this study (Subsection 3.2). A geographical description of major topographic features on Mars is given in Fig. 1. The Martian surface topography computed on a  $1 \times 1$  arc-deg grid varies as much as from  $-8.1$  to  $21.1$  km (see Fig. 2). The most prominent long-wavelength feature is the hemispheric dichotomy (Smith and Zuber, 1996) manifested topographically by the elevated southern hemisphere (the southern highlands) and the lowered northern hemisphere (the northern lowlands) which contributes to about 3.3 km offset between the geometrical and mass centers of the planet. This dichotomy is also evident from their different geological and geo-

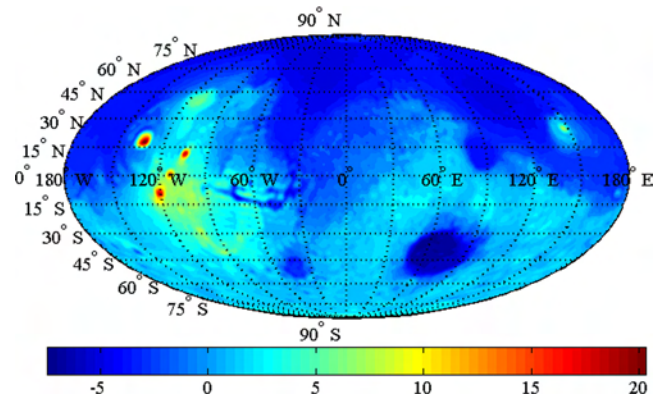


Fig. 2. Martian surface topography (in km).

morphologic compositions. A heavily cratered surface of the southern hemisphere that includes volcanic regions and canyons was formed during the Noachian epoch (Frey et al., 2002). The northern hemisphere is considerably smoother, resurfaced by sedimentary deposits and lava flows during the Hesperian epoch (e.g., Scott and Tanaka, 1986). Hypotheses explaining the hemispheric dichotomy have included one or more massive impacts into the northern hemisphere (Wilhelms and Squyres, 1984), thinning of the northern-hemisphere crust by mantle convection (Wise et al., 1979) and an early period of tectonic-plate recycling (Sleep, 1994).

The medium-to-shorter wavelength topography is dominated by the Tharsis bulge, a vast and complex topographic rise comprising the largest shield volcanoes of Olympus, Ascræus, Arsia and Pavonis Mons. Different explanations of Tharsis formation have been given that include dynamic support of topography by a large mantle plume (Hartman, 1973), regional uplift due to underplating

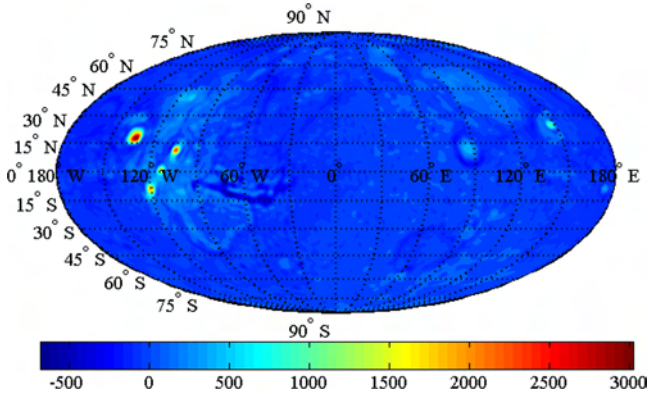


Fig. 3. Martian free-air gravity anomalies (in mGal).

of crustal material derived from the northern hemisphere (Wise et al., 1979), uplift, either due solely to mantle anomalies – thermal and/or compositional (Sleep and Phillips, 1979), or from crustal thickening by intrusion (Phillips et al., 1990) and flexural loading from volcanic construction (Phillips et al., 1990, 2001). A possible scenario of Tharsis evolution comprising three major geological events was proposed by Johnson and Phillips (2005) based on the analysis of magnetic survey.

Tharsis volcanic evolution (with a subsequent crustal loading) resulted in a significant regional tectonism, most prominently manifested by the Valles Marineris rift valleys (Zuber, 2001). The Elysium region in the northern lowlands is another topographic rise shaped by volcanism and faulting, but at a much smaller scale than Tharsis. Mars surface also preserves the record of large impacts that occurred during the Noachian period in the post-accretional phase of heavy bombardment. The largest impact basins are Hellas, Utopia, Argyre and Isidis. Utopia basin has about the same size as Hellas, but is much shallower. This provides the evidence for the thickness of the northern-hemisphere fill (Zuber, 2001). More detailed relief structures comprise numerous smaller impact craters of different age.

### 3.2. Martian (free-air) gravity field

The MRO110B2 is the latest Martian gravity model developed by the Jet Propulsion Laboratory based on 8.5 yrs of the Mars Global Surveyor (MGS) and 6 yrs of the Mars Odyssey (ODY) Doppler and range tracking data. This model also incorporates 2 yrs of low-orbiting Mars Reconnaissance Orbiter (MRO) tracking data (Konopliv et al., 2011). MRO110B2 has a spectral resolution complete to a spherical harmonic degree of 85. The MRO110B2 gravity anomalies computed on a  $1 \times 1$  arc-deg surface grid vary between  $-680$  and  $3095$  mGal (see Fig. 3). This range of gravity values is much larger than that observed in the Earth's gravity field, with most of the free-air gravity anomalies within  $\pm 300$  mGal. Nevertheless, the long-wavelength gravity field of both planets is relatively smooth, which indicates that most of the large-scale topographic features are isostatically compensated (Neumann et al., 2004). This was confirmed also by Phillips and Saunders (1975). They demonstrated that most of the major topographic features of the southern highlands are fully isostatically compensated (see also Frey et al., 2002; and McGovern et al., 2002). The medium-to-higher frequency gravity spectrum is highly spatially correlated with more detailed topography formed by volcanism, regional tectonism and impact craters, which are – in most of the planetary bodies – not fully isostatically compensated (Wieczorek, 2007). Conversely, topographic loads at shorter spatial scales are generally assumed to be supported by the rigidity of the lithosphere. Arkani-Hamed and Riendler (2002), for instance,

demonstrated the existence of large positive crustal density perturbations under Olympus and Tharsis Montes. Their finding indicates that these shield volcanoes are not fully isostatically compensated. This, obviously, has the implication on a maximum resolution up to which the Martian crustal thickness can realistically be recovered merely from gravity field (in the absence of seismic data).

The maximum positive gravity anomalies mark distinctively the locations of Olympus Mons, Tharsis Montes and Alba Patera (e.g., Zuber, 2001; Wieczorek and Zuber, 2004). Almost whole region of the Tharsis province is characterized by large horizontal spatial gravity variations with gravity minima along Valles Marineris. The local gravity high is also seen over Elysium Mons, while the Hellas impact basin is characterized by gravity lows.

### 3.3. Martian Bouguer gravity field

We further computed the Bouguer gravity anomalies using the following expression

$$\Delta g_{n,m}^B = \Delta g_{n,m} - 2\pi G \rho^c H_{n,m}, \quad (8)$$

where  $\Delta g_{n,m}^B$  and  $\Delta g_{n,m}$  are the spherical harmonic coefficients of the Bouguer and free-air gravity anomalies respectively. The spectral Bouguer gravity reduction term  $2\pi G \rho^c H_{n,m}$  was computed from the MOLA topographic coefficients  $H_{n,m}$  (up to degree/order 85).

We adopted the value of  $2900 \text{ kg/m}^3$  to define the average crustal density of Mars. McGovern et al. (2002) found that this average value provided the best fit to a localized admittance over most of the Martian surface when taking into consideration the sub-crustal loading in some specific regions (see also Neumann et al., 2004). Several studies suggest that the crustal density on Mars varies significantly. Wieczorek and Zuber (2004) advocated that the Martian crustal densities range within  $2700$  and  $3100 \text{ kg/m}^3$ . The regional density variations between  $2350$  and  $3350 \text{ kg/m}^3$  were assumed for the rocky crust by McSween (1985) and McKenzie et al. (2002), while the polar layered terrains, up to  $3 \text{ km}$  thick (Smith et al., 1999b), are likely less dense. McGovern et al. (2002) estimated that Tharsis Montes is composed of large crustal densities up to about  $3150 \text{ kg/m}^3$ , while the northern parts of Valles Marineris have possibly a density as low as  $2000 \text{ kg/m}^3$ . McGovern et al. (2002) proposed that the major domical edifices of Tharsis are denser than  $2900 \text{ kg/m}^3$ , although their analysis represented averages over a broader region than a single volcano. Kiefer (2004) inferred local densities exceeding  $3300 \text{ kg/m}^3$  in extinct magma chambers underlying shallower volcanoes such as Nili Patera. The polar caps, composed mainly of  $\text{H}_2\text{O}$  ice coated with a thin layer of  $\text{CO}_2$  ice and dust, have densities similar to that of water ice (cf. Smith et al., 1999b).

In our study, these Martian crustal density variations were disregarded due to difficulties with their spatial localization in the absence of digital density model. Since the density uncertainties propagate proportionally to errors in computed values of the Bouguer gravity anomalies and the Moho depths, the relative errors typically less than 10% are to be expected in the gravimetrically determined Moho geometry if referring to the crustal density variations mostly within  $2700$  to  $3100 \text{ kg/m}^3$ . Obviously, even larger relative errors in the Moho geometry could be expected under more complex crustal structures.

The Bouguer gravity anomalies computed on a  $1 \times 1$  arc-deg surface grid vary between  $-897$  and  $898$  mGal (see Fig. 4). The application of the Bouguer reduction significantly decreases the gravity range, from  $3775$  mGal (for the free-air gravity anomalies) to only  $1795$  mGal (for the Bouguer gravity anomalies). The most prominent feature in the map of the Bouguer gravity anomalies is the hemispheric dichotomy. It propagates into the first-degree

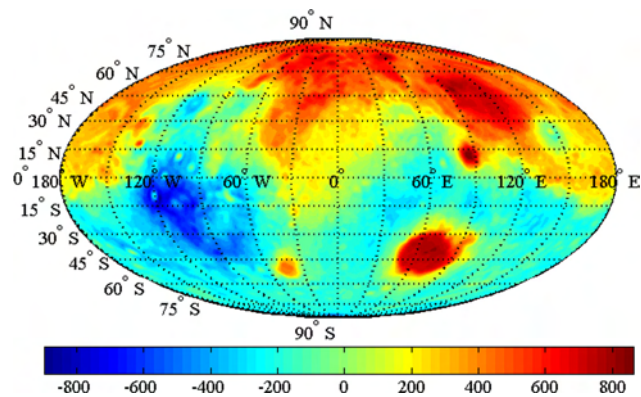


Fig. 4. Martian Bouguer gravity anomalies (in mGal).

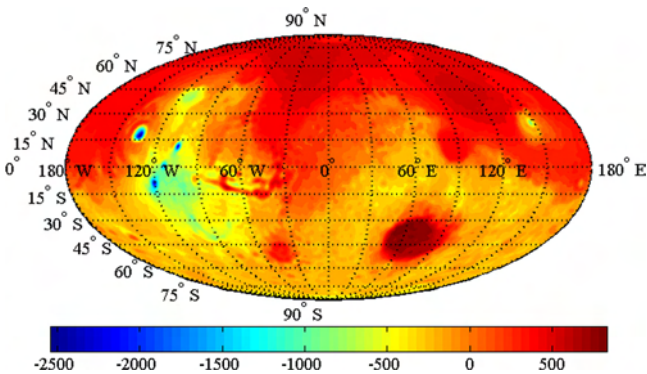


Fig. 5. Martian Bouguer gravity reduction (in mGal).

zonal harmonic term (Neumann et al., 2004) due to the mass excess in the northern hemisphere (with the prevailing positive gravity anomalies) and the mass deficit in the southern hemisphere (with mostly negative gravity anomalies). In addition, the signatures of variable topography and regional geological structure are superposed over this prevailing pattern at medium-to-higher frequencies of the Bouguer gravity spectrum. The largest positive values of the Bouguer gravity anomalies mark distinctively locations of Hellas, Isidis, Utopia and Argyre basins. The largest (in magnitude) negative Bouguer gravity anomalies are distributed over Tharsis. The largest negative values of the Bouguer gravity anomalies on the Earth's surface correspond with the highest elevations in Himalaya and Tibet. It is interesting to see that on Mars such phenomenon is absent, meaning that the largest negative values are not seen at Olympus Mons and Tharsis Montes. To explain this we plotted the map of the Bouguer gravity reduction in Fig. 5. As seen from the comparison of Figs. 3 and 5, the free-air gravity anomalies at the highest elevations on Mars are much larger (in absolute sense) than the Bouguer gravity reduction; the free-air gravity anomalies exceed 2500 mGal while the Bouguer gravity reduction is less than 2500 mGal. Two more isolated local gravity lows at the northern hemisphere are in Elysium Mons and Alba Patera. For a more detailed geological classification of the Bouguer gravity anomalies on Mars we refer readers to study by Neumann et al. (2004). We note that they presented the Bouguer gravity map corrected for the first- and zero-degree harmonics.

#### 4. Results

The MOLA topographic and MRO110B2 gravity models were used to determine the Martian crustal thickness (Subsection 4.1) and the sub-crustal stress (Subsection 4.2) with a spectral resolution complete to a spherical harmonic degree of 85 (which corresponds to a half-wavelength of 2.1 arc-deg, or about 125 km on

equator). All computations were realized on a  $1 \times 1$  arc-deg spherical grid.

##### 4.1. Martian crustal thickness

Since seismic measurements were not yet conducted on Mars, several different methods (and constraining parameters) have been applied to estimate the Martian crustal thickness. Bills and Nerem (1995) estimated the mean crustal thickness to be between 50 and 200 km. Sohl and Spohn (1997) used geochemical arguments to estimate that the mean crustal thickness is within the range of 100 to 250 km. Norman (1999) estimated that less than 45 km of crust could be geochemically enriched. Viscous relaxation studies of Zuber et al. (2000) and Nimmo and Stevenson (2001) indicated that the average crustal thickness is somewhere between 50 and 100 km. Nimmo (2002) inferred a maximum possible crustal thickness of 75 km across the dichotomy boundary with the global average of about 55 km. Turcotte et al. (2002) estimated that the crustal thickness around Hellas basin exceeds 90 km. Studying a spectral-admittance of major highland features, McGovern et al. (2002) estimated the lower limit of the average crustal thickness at 32 km. Wiczeorek and Zuber (2004) suggested an average thickness of  $50 \pm 12$  km from the review of previous geophysical and geochemical studies.

The first reliable model of the Martian crustal thickness was compiled by Zuber et al. (2000) by analyzing the gravity field derived from the preliminary MGS tracking (Smith et al., 1999a) and topographic information from MOLA and MGS. They reported an average crustal thickness of 45 km. They also estimated that the minimum thickness of 3 km is beneath Isidis basin, and the maximum thickness of 92 km occurs in the Syria Planum region of Thaumasia. Neumann et al. (2004) reported the Martian crustal thickness variations between 5.8 and 102 km with the minima under Hellas and Isidis basins and the maxima under Tharsis major volcanoes. They also proposed that the northern lowlands are presumably underlain by a thinner crust averaging about 32 km, whereas the southern highlands are underlain by a thicker crust averaging about 58 km.

We computed the Martian crustal thickness by solving the VMM problem. The isostatic compensation attraction and the Moho depths were determined for a uniform Moho density contrast of  $600 \text{ kg/m}^3$  (Neumann et al., 2004). This density contrast is representative for the olivine upper mantle of  $3500 \text{ kg/m}^3$  derived based on the geochemical analysis of shergottite, nakhlite and chassigny (SNC) class of meteorites (Sohl and Spohn, 1997). It is worth mentioning that some geochemical models imply pyroxene as a major mineral in the olivine–pyroxene–garnet chemical composition of the Martian upper mantle. The choice of a different value of the Moho density contrast will, however, not change the Moho geometry (only a mean Moho depth).

The Martian crustal thickness according to our estimate varies between 12.3 and 89.5 km (see Fig. 6). This range (of 77.2 km) is about 20% smaller than the crustal thickness variations (of 96.2 km) found by Neumann et al. (2004). Compared to their crustal model, our result underestimated the crustal thickness in the Tharsis province and overestimated the crustal thickness under major impact basins. This is explained by applying the VMM isostatic model instead of Airy's compensation scheme. Neumann et al. (2004), however, modeled more accurately the actual crustal structures by using different density values for specific geological formations on Mars. According to our result the average crustal thickness is 46.4 km. This average value is within the interval of previous estimates reported by Zuber et al. (2000), Neumann et al. (2004) and Wiczeorek and Zuber (2004).

The most prominent feature in the crustal geometry (Fig. 6) is a significant contrast between a thicker crust underlying the south-

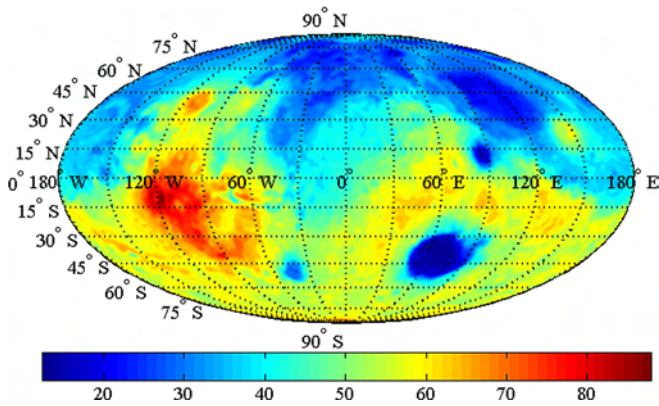


Fig. 6. Martian crustal thickness (in km).

ern highlands and a thinner crust under the northern lowlands. The crustal thickness of the northern lowlands is typically less than 40 km. The crustal thickness under most of the heavily cratered southern highlands exceeds 45 km, except for much thinner crust under Hellas and Argyre basins, with the crustal thickness decreasing to less than 30 km under Argyre basin and as low as 13 km under Hellas basin. Similarly, Utopia and Isidis basins on the northern hemisphere are characterized by a very thin crust, with the thickness locally decreasing to 20 and 14 km respectively. This significant crustal thinning is explained by a Moho uplift after impact (Neumann et al., 1996) and a subsequent modification by volcanic and sedimentary surface loads (Buczowski and Cooke, 2004), which is most prominent in Utopia basin with thick sedimentary deposits and lava covers. The crustal thickness in the Tharsis province typically exceeds 70 km. This large crustal thickness is attributed to a crustal flexure due to a load of volcanic accumulations, which is manifested by a Moho deepening extending under a broader area of the Tharsis province. The crust under the broad Arabia is thickening more gradually. In Arabia and Elysium regions the dichotomy boundary is compensated by a crustal thickness variation, with more pronounced relief along the Moho than at the surface (see also Neumann et al., 2004).

#### 4.2. Martian sub-crustal stress

We used the gravimetric Moho depths to determine the Martian sub-crustal stress (according to Eq. (2)) with a complementary study of the stress field in the Tharsis region. We also investigated a spectral behavior of the sub-crustal stress field in order to be able to separate and study the (long-wavelength) stress component.

##### 4.2.1. Global stress field

The horizontal stress vectors and their intensity are shown in Fig. 7. Most of the Martian sub-crustal stress intensity is accumulated in the Tharsis region. The maximum stress intensity (up to 280 MPa) is detected at a location of Olympus Mons. The local maxima of stress intensity also coincide with Ascraeus, Arsia and Pavonis Mons. Another pronounced stress anomalies are distributed along Valles Marineris. Despite some geological similarities between the Elysium and Tharsis regions, the stress intensity at Elysium Mons is much smaller (less than 120 MPa). Moreover, the stress distribution there is without any spatial complexity that is seen in Tharsis. A more detailed analysis of the stress field in the Tharsis region is postponed until Subsubsection 4.2.7.

##### 4.2.2. Signature of impact craters

Elsewhere, the stress intensity is typically much smaller (or completely absent) with slightly enhanced contours of four major

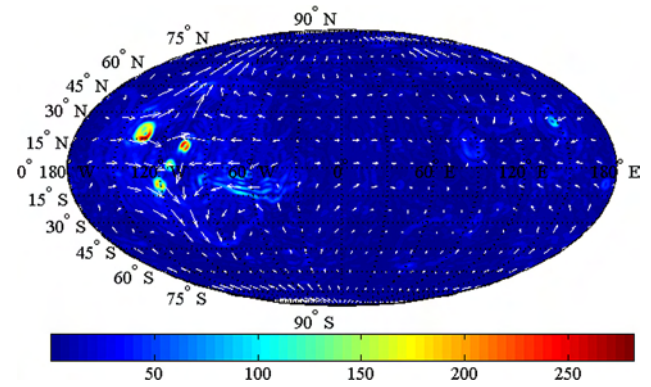


Fig. 7. Martian sub-crustal stress field: the horizontal stress vectors and their intensity (in MPa).

impact basins (Isidis, Hellas, Argyre and Utopia). These signatures are explained by a crustal extrusion after impact, followed by a mantle inflow in response to the isostatic rebalance of the modified crust. This Moho uplift generates the maximum horizontal stress intensity around the impact crater. The pronounced stress intensity at these locations indicates that impact basins are not fully isostatically compensated. The stress field thus likely remains present even a very long time after the impact event, until these basins are eventually modified by volcanic or sedimentary covers. This is evident in Utopia basin with large sedimentary and lava deposits, responsible for the additional crustal thickening and a subsequent decreasing of the stress intensity (compared to more pronounced stress intensity around Hellas basin) due to a partial isostatic rebalance.

##### 4.2.3. Signature of hemispheric dichotomy

Except for the isolated stress anomaly along the northern part of Alba Patera, margins dividing the southern highlands from the northern lowlands are not pronounced. The signature of the hemispheric dichotomy is thus absent. This finding might be explained by the fact that, except for more detailed topographic features, the southern highlands are isostatically fully compensated (Frey et al., 2002; McGovern et al., 2002).

##### 4.2.4. Signature of ice load

There is also no evidence of the stress field associated to a crustal load of polar ice caps. Since these ice caps are geologically young, the isostatic adjustment to a changing load might be incomplete (Neumann et al., 2004). Moreover, the undergoing lithospheric and mantle relaxation due to ice load takes place over time scales of  $10^5$ – $10^7$  yrs (Johnson et al., 2000). As a consequence, the Moho deepening under polar ice caps is likely in its early stage.

##### 4.2.5. Spectral analysis of stress field

As stated in Subsubsection 4.2.1, the western hemisphere has regions of significantly more pronounced stress intensity than the eastern hemisphere. This asymmetry might be somehow related to the (second-order) dichotomy of Tharsis volcanic formation (Neumann et al., 2004). This implies a possible long-wavelength signature in the stress field. Moreover, the sub-crustal stress field on Mars is manifested by different spatial distributions and intensities which are specific for tectonic features, crustal loading of volcanic accumulations and impact basins (see Fig. 7). These stress anomalies propagate into the medium-to-higher frequency spectrum.

To examine the signal spectrum of the Martian sub-crustal stress we computed the degree variances  $\sigma_n^2$  and the respective

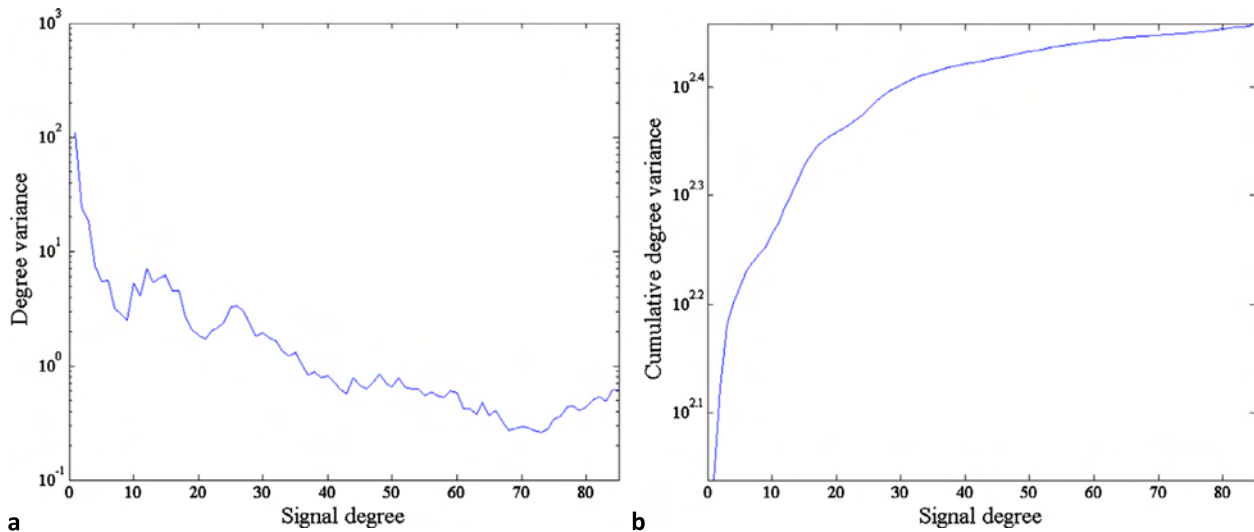


**Fig. 8.** Signal spectrum of the Martian stress field: (a) the degree variances, and (b) the cumulative degree variances of the stress intensity (in MPa<sup>2</sup>).

cumulative degree variances  $\Theta_{\bar{n}}$  from the coefficients  $S_{n,m}$  of the stress intensity as follows

$$\sigma_{\bar{n}}^2(S) = \sum_{m=-n}^n S_{n,m}^2, \quad \Theta_{\bar{n}}(S) = \sum_{n=0}^{\bar{n}} \sigma_{\bar{n}}^2(S). \quad (9)$$

As seen in Fig. 8, the maximum stress intensity is distributed at the long-wavelength spectrum (up to degree 5), while attenuates at the medium-to-higher frequency spectrum up to degree of about 70. Above this degree, the stress intensity again magnifies. Additional oscillations in spectral pattern are seen at the medium wavelengths (with the amplified signal above degree 10 and around degree 25, and signal lows at degrees 8 and 20).

Most of the horizontal stress intensity is generated by crustal structures which are not fully isostatically compensated. This is evident, for instance, in the presence of the stress anomalies around volcanoes of Olympus and Elysium Mons and Tharsis Montes. These stress anomalies are propagated to the higher-frequency spectrum (above degree 70). The stress field of the isostatically uncompensated crustal structures underlying impact craters, on the other hand, occupies mainly the medium wavelengths. The stress field along Valles Marineris has a broader spectral signature. The long-wavelength stress field is investigated in the next paragraph.

#### 4.2.6. Long-wavelength stress field

The long-wavelength part of the Martian sub-crustal stress field, which includes spherical harmonics up to degree 5, is shown in Fig. 9. Most of the stress anomalies are distributed in the Tharsis region, showing some circular symmetry with the minimum intensity in its center and an increasing intensity towards Tharsis margins. This circular pattern of the stress anomalies is very similar to that we observe around major volcanoes. This stress field is thus likely caused by a crustal load of the Tharsis bulge. Moreover, the orientation of stress vectors is systematically convergent in the prime-vertical direction, while divergent in the meridional direction. The crustal load is – in this case – manifested by the prime-vertical compressional stress coupled by the meridional tensional stress.

Whereas the signature of the hemispheric dichotomy is absent, the signature of the additional Tharsis dichotomy is clearly recognized in the long-wavelength stress field. There are possibly two reasons which might explain this finding. The Tharsis region is not fully isostatically compensated due to either its size or its age (or combination of both these factors). A time factor implies that

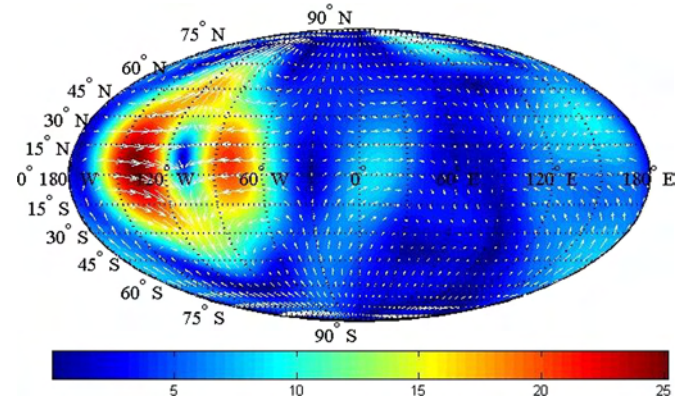


**Fig. 9.** Long-wavelength part (up to degree 5) of the Martian sub-crustal stress field: The horizontal stress vectors and their intensity (in MPa).

the geological event responsible for creating the hemispheric dichotomy occurred earlier than Tharsis formation. This assumption agrees with the theory of Phillips et al. (2001). They proposed a single mechanism for the highland crustal formation, with modification by the Hellas impact that resulted to additional construction of Tharsis, as the basin dips into the trough formed by and circumferential to the Tharsis load. The alternative theory which supports our assumption was proposed by Zhong and Zuber (2001). They suggested that the thick crustal structure underlying the southern lowlands was formed during an early phase of mantle convection, which involved a plume upwelling that formed due to viscosity stratification in the mantle. Roberts and Zhong (2007) suggested that since the Tharsis region has a dichotomy asymmetry on its own with more volcanism in the western hemisphere than the eastern hemisphere, that this asymmetry, which is about 90 arc-deg offset from the topographic dichotomy, may be reason to support the mantle plume migration theory that started at the South Pole and migrated to about 90 arc-deg toward the dichotomy boundary at the equator (see also Sramek and Zhong, 2012).

#### 4.2.7. Tharsis stress field

As seen in Fig. 10, the signature of Tharsis dichotomy in the stress field is superimposed by more detailed stress patterns around Tharsis major volcanoes and along Valles Marineris. A circularly distributed stress around Tharsis major volcanoes is closely spatially correlated with the topography. Under higher elevations we observe minima of the horizontal sub-crustal stress coupled by

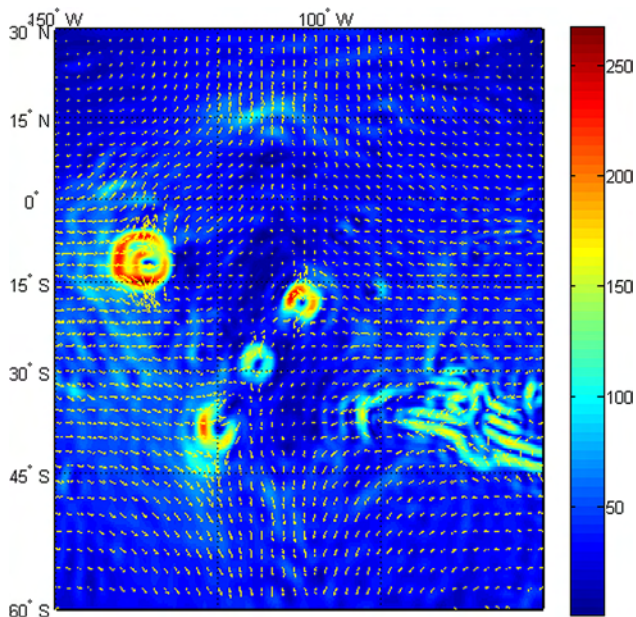


Fig. 10. Sub-crustal stress vectors and their intensity (in MPa) in Tharsis region.

stress maxima under lower elevations. A similar pattern is seen around Elysium Mons (see Fig. 7). Minima of the stress intensity under volcanic centers indicate the presence of tensional stress while compressional stress corresponds with maxima of the stress intensity. By analogy with the signature of the Tharsis dichotomy, this pattern could be explained by an isostatic imbalance caused by a crustal load of volcanic accumulations. Alternatively, it could preserve the signature of earlier stage of volcanic formations related to buoyancy and a localized reduction of elastic strength of the lithosphere (due to thermal gradient between volcanism and background progressive cooling). Despite the sub-crustal stress could not directly explain surface geomorphologic features, there are some similarities with regional tectonic formations of grabens, wrinkle ridges and peripheral belt. The graben formations require extensional stresses circumferential to volcanoes while wrinkle ridges and peripheral belt are related to horizontal shortening. Dimitrova et al. (2006) demonstrated that the deviatoric stress associated with the horizontal gravity gradients shows deviatoric extension over topographically high areas transitioning to deviatoric compression at topographically low areas. They also showed that, at shorter wavelengths, the deviatoric stress closely reproduces most of the normal faults in Tharsis regions and wrinkle ridges circumferential to Tharsis. The distribution of the stress anomalies along Valles Marineris has a more complex pattern. The most prominent is a change of the stress intensity across rift valleys with minima under valleys (corresponding to tensional stress) coupled by local maxima on both sides (extensional stress). As discussed before, this stress pattern is likely related to a regional tectonism caused by a crustal loading of Tharsis.

## 5. Conclusions

We have applied the method of Eshagh and Tenzer (2014) to compute the sub-crustal stress on Mars. Compared to the Runcorn (1964) formulae, this method allows computing the stress field with a spectral resolution that is compatible with the currently available global gravity and crustal structure models of most of the planetary bodies. For Mars, we computed the stress field up to a spherical harmonic degree of 85, which corresponds to a spectral resolution of the MRO110B2 Martian gravity model.

Furthermore, we have solved the VMM inverse problem of isostasy for a determination of the crustal thickness based on adopting a global compensation principle. Since the isostatic mass balance depends on loading and effective elastic thickness, rigidity, rheology of the lithosphere and viscosity of the asthenosphere, we expect that a regional isostatic scheme should reproduce more realistically the actual compensation mechanisms than the Airy local isostatic model used in previous studies.

We have identified various sources of the Martian sub-crustal stress, which include: (i) crustal load of volcanic accumulations, (ii) regional tectonism and (iii) impact of meteorites. The crustal load of Tharsis volcanic formations is likely also responsible for a regional tectonism of Valles Marineris. In contrast, the stress distribution around major impact basins was explained by crustal extrusion after impact, followed by a Moho uplift.

Among these three categories, the crustal loading generates the maximum intensity of the sub-crustal stress on Mars. This is evident in the most prominent signatures of crustal loads of Tharsis major volcanoes (Olympus, Ascraeus, Arsia and Pavonis Mons) and that of Elysium Mons. These shield volcanoes are thus not fully isostatically compensated, the interpretation which agrees with the finding of Arkani-Hamed and Riendler (2002).

In addition to these localized stress anomalies, the crustal load of Tharsis volcanic accumulations generates a large-scale stress field, which distinctively marks the Tharsis dichotomy. In contrast, the signature of the hemispheric dichotomy is absent. The incomplete isostatic compensation of the Tharsis bulge might be explained by its more recent formation compared to the (fully compensated) southern highlands. This assumption agrees with the theory of a single highland formation followed by the additional construction of Tharsis by the Hellas impact proposed by Phillips et al. (2001) as well as with the mantle plume migration theory of Roberts and Zhong (2007) and Zhong (2009).

Despite the fact that the crustal load is likely responsible for most of the Martian sub-crustal stress, the signature of polar ice load is missing. A possible explanation of this finding was given by Neumann et al. (2004). They suggested that the polar ice caps on Mars are geologically relatively young, while the isostatic adjustment to a changing load takes place over time scales of  $10^5$ – $10^7$  yrs (Johnson et al., 2000).

The geomorphological features of Valles Marineris and its specific stress distribution are likely explained by a regional tectonism, which is related to a crustal load of the Tharsis Bulge. This is in agreement with more recent theories of the Valles Marineris formation attributed to either tensional fracturing (Tanaka and Golombek, 1989) or regional extensional tectonism (Banerdt et al., 1992). A better understanding of the processes which formed Valles Marineris is, however, still open to investigation.

The stress distribution on Mars and its possible origin are quite different from those observed on Earth. Tenzer and Eshagh (in press) and Eshagh and Tenzer (2014) demonstrated that most of the sub-crustal stress on Earth is generated by active global tectonics. They also identified the additional, but much localized stress anomalies caused by a crustal loading of volcanic islands in the vicinity of hotspots. On Mars, the situation is opposite. Except for the regional tectonism of Valles Marineris, the signature of active global tectonics is absent. The Martian lithosphere was thus not fractured by tectonic forces into individual plates. This finding supports the theory of a single lithospheric plate on Mars (which rotated due to polar wander) proposed by Zhong (2009). We have also demonstrated that most of the Martian sub-crustal stress is generated by a crustal load of volcanic accumulations, which is likely also responsible for a regional tectonism along Valles Marineris. Another significant difference between the stress fields of these two planets is the signature of impacts on Mars and its absence on Earth.

## Acknowledgements

The MOLA topographic data and the MRO110B2 gravity model used in this study are made available through the Geosciences Node of NASA's Planetary Data System archives (<http://pds-geosciences.wustl.edu>).

## References

- Arkani-Hamed, J., Riendler, L., 2002. Stress differences in the Martian lithosphere: constrains on the thermal state of Mars. *J. Geophys. Res.* 107 (E12), 5119. <http://dx.doi.org/10.1029/2002JE001851>.
- Banerdt, W.B., Golombek, M.P., Tanaka, K.L., 1992. Stress and tectonics on Mars. In: Kieffer, H.H., Jakosky, B.M., Snyder, C.W., Matthews, M.S. (Eds.), *Mars*. Univ. of Arizona Press, Tucson, AZ, pp. 249–297.
- Bills, B.G., Nerem, R.S., 1995. A harmonic analysis of Martian topography. *J. Geophys. Res.* 100, 26,317–26,326.
- Buczowski, D.L., Cooke, M.L., 2004. Formation of double-ring circular grabens due to volumetric compaction over buried impact craters: implications for thickness and nature of cover material in Utopia Planitia, Mars. *J. Geophys. Res.* 109 (E2), E02006. <http://dx.doi.org/10.1029/2003JE002144>.
- Dimitrova, L.L., Holt, W.E., Haines, A.J., Schiltz, R.A., 2006. Toward understanding the history and mechanisms of Martian faulting: the contribution of gravitational potential energy. *Geophys. Res. Lett.* 33, L08202. <http://dx.doi.org/10.1029/2005GL025307>.
- Eshagh, M., Tenzer, R., 2014. Sub-crustal stress determined using gravity and crust structure models. *Comput. Geosci.* 19 (1), 115–125. <http://dx.doi.org/10.1007/s10596-014-9460-9>.
- Frey, H.V., Roark, J.H., Shockey, K.M., Frey, E.L., Sakimoto, S.E.H., 2002. Ancient lowlands on Mars. *Geophys. Res. Lett.* 29 (10), 1384. <http://dx.doi.org/10.1029/2001GL013832>.
- Hartman, W.K., 1973. Martian cratering: 4. Mariner 9 initial analysis of cratering chronology. *J. Geophys. Res.* 78, 4096–4116.
- Johnson, C.L., Solomon, S.C., Head, J.W., Phillips, R.J., Smith, D.E., Zuber, M.T., 2000. Lithospheric loading by the north polar cap of Mars. *Icarus* 144, 313–328.
- Johnson, C.L., Phillips, R.J., 2005. Evolution of the Tharsis region of Mars: insights from magnetic field observations. *Earth Planet. Sci. Lett.* 230, 241–254.
- Kiefer, W.S., 2004. Gravity evidence for an extinct magma chamber beneath Syrtis Major, Mars: a look at the magmatic plumbing system. *Earth Planet. Sci. Lett.* 222, 349–361.
- Konopliv, A.S., Asmar, S.W., Folkner, W.M., Karatekin, Ö., Nunes, D.C., Smrekar, S.E., Yoder, C.F., Zuber, M.T., 2011. Mars high resolution gravity fields from MRO, Mars seasonal gravity, and other dynamical parameters. *Icarus* 211, 401–428.
- McGovern, P.J., Solomon, S.C., Smith, D.E., Zuber, M.T., Simons, M., Wieczorek, M.A., Phillips, R.J., Neumann, G.A., Aharonson, O., Head, J.W., 2002. Localized gravity/topography admittance and correlation spectra on Mars: implications for regional and global evolution. *J. Geophys. Res.* 107 (E12), 5136. <http://dx.doi.org/10.1029/2002JE001854>.
- McKenzie, D., Barnett, D.N., Yuan, D., 2002. The relationship between Martian gravity and topography. *Earth Planet. Sci. Lett.* 195, 1–16.
- McSween, H.Y., 1985. SNC meteorites: clues to Martian petrologic evolution? *Rev. Geophys.* 23, 391–416.
- Neumann, G.A., Zuber, M.T., Smith, D.E., Lemoine, F.G., 1996. The lunar crust: global structure and signature of major basins. *J. Geophys. Res.* 101, 16841–16863.
- Neumann, G.A., Zuber, M.T., Wieczorek, M.A., McGovern, P.J., Lemoine, F.G., Smith, D.E., 2004. Crustal structure of Mars from gravity and topography. *J. Geophys. Res.* 109, E08002. <http://dx.doi.org/10.1029/2004JE002262>.
- Nimmo, F., Stevenson, D.J., 2001. Estimates of Martian crustal thickness from viscous relaxation of topography. *J. Geophys. Res.* 106, 5085–5098.
- Nimmo, F., 2002. Admittance estimates of mean crustal thickness and density at the Martian hemispheric dichotomy. *J. Geophys. Res.* 107 (E11), 5117. <http://dx.doi.org/10.1029/2000JE001488>.
- Norman, N.D., 1999. The composition and thickness of the crust of Mars estimated from rare earth elements and neodymium-isotopic composition of Martian meteorites. *Meteorit. Planet. Sci.* 34, 439–449.
- Phillips, R.J., Saunders, R.S., 1975. The isostatic state of Martian topography. *J. Geophys. Res.* 80, 2893–2898.
- Phillips, R.J., Sleep, N.H., Banerdt, W.B., 1990. Permanent uplift in magmatic systems with application to the Tharsis region of Mars. *J. Geophys. Res.* 95, 5089–5100.
- Phillips, R.J., Zuber, M.T., Solomon, S.C., Golombek, M.P., Jakosky, B.M., Banerdt, W.B., Smith, D.E., Williams, R.M.E., Hynek, B.M., Aharonson, O., Hauck II, S.A., 2001. Ancient geodynamics and global-scale hydrology on Mars. *Science* 291, 2587–2591.
- Roberts, J.H., Zhong, S., 2007. The cause for the north–south orientation of the crustal dichotomy and the equatorial location of Tharsis on Mars. *Icarus* 190, 24–31.
- Runcorn, S.K., 1964. Satellite gravity measurements and laminar viscous flow model of the Earth mantle. *J. Geophys. Res.* 69 (20), 4389–4394.
- Scott, D.H., Tanaka, K.L., 1986. Geologic map of the western equatorial region of Mars. *US Geol. Survey Map I-1802-A*.
- Sjöberg, L.E., 2009. Solving Vening Meinesz–Moritz inverse problem in isostasy. *Geophys. J. Int.* 179, 1527–1536.
- Sleep, N.H., Phillips, R.J., 1979. An isostatic model for the Tharsis province. *Geophys. Res. Lett.* 6, 803–806.
- Sleep, N.H., 1994. Martian plate tectonics. *J. Geophys. Res.* 99, 5639–5655.
- Smith, D.E., Zuber, M.T., 1996. The shape of Mars and the topographic signature of the hemispheric dichotomy. *Science* 271, 184–188.
- Smith, D.E., Sjogren, W.L., Tyler, G.L., Balmino, G., Lemoine, F.G., Konopliv, A.S., 1999a. The gravity field of Mars: results from Mars global surveyor. *Science* 286, 94–96.
- Smith, D.E., Zuber, M.T., Solomon, S.C., Phillips, R.J., Head, J.W., Garvin, J.B., Banerdt, W.B., Muhleman, D.O., Pettengill, G.H., Neumann, G.A., Lemoine, F.G., Abshire, J.B., Aharonson, O., Brown, C.D., Hauck, S.A., Ivanov, A.B., McGovern, P.J., Zwally, H.J., Duxbury, T.C., 1999b. The global topography of Mars and implications for surface evolution. *Science* 284, 1495–1503.
- Sohl, F., Spohn, T., 1997. The interior structure of Mars: implications from SNC meteorites. *J. Geophys. Res.* 102, 1613–1635.
- Sramek, O., Zhong, S., 2012. Martian crustal dichotomy and Tharsis formation by partial melting coupled to early plume migration. *J. Geophys. Res.* 117, E01005. <http://dx.doi.org/10.1029/2011JE003867>.
- Tanaka, K.L., Golombek, M.P., 1989. Martian tension fractures and the formation of grabens and collapse features at Valles Marineris. In: *Proceedings of the 19th Lunar and Planetary Science Conference*, pp. 383–396.
- Tenzer, R., Eshagh, M., in press. Subduction generated sub-crustal stress in Taiwan. *Terr. Atmos. Ocean. Sci.* [http://dx.doi.org/10.3319/TAO.2014.12.04.01\(T\)](http://dx.doi.org/10.3319/TAO.2014.12.04.01(T)).
- Turcotte, D.L., Scherbakov, R., Malamud, B.D., Kucinskis, A.B., 2002. Is the Martian crust also the Martian elastic lithosphere? *J. Geophys. Res.* 107 (E11), 5091. <http://dx.doi.org/10.1029/2001JE001594>.
- Turtle, E.P., Melosh, H.J., 1997. Stress and flexural modeling of the Martian lithospheric response to Alba Patera. *Icarus* 126 (1), 197–211.
- Wieczorek, M.A., Zuber, M.T., 2004. The thickness of the Martian crust: improved constraints from geoid-to-topography ratios. *J. Geophys. Res.* 109 (E1), E01009. <http://dx.doi.org/10.1029/2003JE002153>.
- Wieczorek, M.A., 2007. The gravity and topography of the terrestrial planets. In: Schubert, G. (Ed.), *Treatise on Geophysics*, vol. 10. Elsevier–Pergamon, Oxford, UK, pp. 165–206.
- Wilhelms, D.E., Squyres, S.W., 1984. The Martian hemispheric dichotomy may be due to a giant impact. *Nature* 309, 138–140.
- Wise, D.U., Golombek, M.P., McGill, G.E., 1979. Tectonic evolution of Mars. *J. Geophys. Res.* 84, 7934–7939.
- Zhong, S., 2009. Migration of Tharsis volcanism on Mars caused by differential rotation of the lithosphere. *Nat. Geosci.* 2, 19–23. <http://dx.doi.org/10.1038/NCEO392>.
- Zhong, S., Zuber, M.T., 2001. Degree-1 mantle convection and the crustal dichotomy on Mars. *Earth Planet. Sci. Lett.* 189, 75–84.
- Zuber, M.T., Solomon, S.C., Phillips, R.J., Smith, D.E., Tyler, G.L., Aharonson, O., Balmino, G., Banerdt, W.B., Head, J.W., Johnson, C.L., Lemoine, F.G., McGovern, P.J., Neumann, G.A., Rowlands, D.D., Zhong, S., 2000. Internal structure and early thermal evolution of Mars from Mars global surveyor topography and gravity. *Science* 287, 1788–1793.
- Zuber, M.T., 2001. The crust and mantle of Mars. *Nature* 412 (12), 220–227.